Survey of the H-mode power threshold and transition physics studies in ASDEX Upgrade

F. Ryter[1], S.K. Rathgeber[1], L. Barrera Orte[1], M. Bernert[1], G.D. Conway[1], R. Fischer[1], T. Happel[1], B. Kurzan[1], R.M. McDermott[1], A. Scarabosio[1], W. Suttrop[1], E. Viezzer[1], M. Willensdorfer[2], E. Wolfrum[1] and the ASDEX Upgrade Team[1]

[1] Max-Planck-Institut für Plasmaphysik, EURATOM Association, D-85748 Garching, Germany

[2] Institute of Applied Physics, Vienna University of Technology, EURATOM-ÖAW, Vienna, Austria

E-mail: ryter@ipp.mpg.de

Abstract. An overview of the H-mode threshold power in ASDEX Upgrade which addresses the impact of the tungsten versus graphite wall, the dependences upon plasma current and density, as well as the influence of the plasma ion mass is given. Results on the H-L back transition are also presented. Dedicated L-H transition studies with electron heating at low density, which enable a complete separation of the electron and ion channels, reveal that the ion heat flux is a key parameter in the L-H transition physics mechanism through the main ion pressure gradient which is itself the main contribution to the radial electric field and the induced flow shearing at the edge. The electron channel does not play any role. The 3D magnetic field perturbations used to mitigate the ELMs are found to also influence the L-H transition and to increase the power threshold. This effect is caused by a flattening of the edge pressure gradient in the presence of the 3D fields such that the L-H transitions with and without perturbations occur at the same value of the radial electric field well, but at different heating powers.

1. Introduction

The H-mode, which will be the base line scenario for ITER, is obtained above a certain heating power threshold, P_{L-H}, at which the L-H transition occurs. The L-H transition and its threshold have been investigated during the last decades in most fusion devices. The multi-machine international threshold database, described in [1], is used to deduce scaling expressions for the H-mode threshold power and the analysis from 2008 yielded the latest and widely used ITPA threshold scaling which for deuterium reads, [2]:

$$P_{scal} = 0.049\,\bar{n}_e{}^{0.72} B_T{}^{0.80} S^{0.94} \tag{1}$$

where $\bar{n}_e$ is the line-averaged density in $10^{20}\mathrm{m}^{-3}$, B_T the magnetic field in T, and S the plasma surface area in m^2. This scaling expression is used to predict P_{L-H} in future devices and to normalize the experimental values of P_{L-H} for comparison between devices or different discharges in a single machine. It should be underlined that as the B_T dependence is well reproduced across the whole database, independently of device and plasma conditions, in some of the analyses presented below we use it to compare discharges with different B_T values over a restricted range. It should also be noted that the radiation losses from the volume inside the separatrix are not subtracted. Expression 1 has been deduced from discharges with low threshold, generally labeled as "favorable" occurring in deuterium plasmas with a magnetic configuration for which the ion ∇B drift is directed toward the X-point. It is also known for decades that for the hydrogen isotopes (H, D and T) P_{L-H} varies with the ion mass as M_i^{-1}, [3], such that it is 2 times higher in hydrogen and 2/3 lower in tritium as compared to deuterium. In contrast, the case of helium (^{4}He throughout this paper) is less clear: in some devices the threshold is reported to be up to 40% higher in helium than in deuterium but is also found to be very close to the deuterium threshold, in particular as density is increased. An overview of these results is provided by joint experiments carried out in the frame of the ITPA Transport and Confinement Group and reported in [4]. The isotope effect is important for predictions of the non-nuclear phase of ITER which will be carried out in hydrogen and helium plasmas. Further dependences have also been reported concerning the position of the

magnetic configuration with respect to the divertor geometry, [5, 6, 7, 8], as well as the impact of the toroidal rotation, [9]. None of these three effects have been found in ASDEX Upgrade, so far, and these topics are not further discussed here.

During the last decade, the graphite plasma facing components in ASDEX Upgrade have been gradually replaced by tungsten-coated elements and the complete replacement of carbon by tungsten was achieved in 2007, [10, 11, 12, 13]. This change has induced a reduction of P_{L-H} by 25%, [14, 15], and is described in more detail below. Also at JET the recent change to a full metallic wall resulted in a reduction of P_{L-H}, [16].

The application of 3D magnetic field perturbations (MPs) is nowadays widely used to mitigate the edge localized modes (ELMs). This also impacts P_{L-H} and, in most of the devices turning on the MPs causes an increase of P_{L-H}, as reported for MAST [17], DIII-D [6], NSTX [18] and ASDEX Upgrade, [19]. In ITER, large ELMs must be avoided, which implies that the ELM mitigation system must be turned on before, or at the latest immediately after the L-H transition. As the available heating power in ITER will not be much higher than the presently predicted P_{L-H}, it is important to assess quantitatively to what extent the MPs might affect the threshold and under which conditions.

Not only the L-H transition is important for ITER, but also the H-L "back-transition" which has been studied much less, so far. The H-L transition has also been addressed in our studies. It is particularly important to know whether, once in the H-mode, the plasma can remain in this regime with less power than predicted by P_{scal}. This property is generally expressed by the power hysteresis defined as the ratio of the power at which the H-L transition occurs to the L-H threshold power, P_{H-L}/P_{L-H}.

It has been largely demonstrated that the physics mechanism of the L-H and H-L transitions takes place at the very edge of the plasma. Over the years, numerous models have been proposed to explain the L-H transition, see e.g. review [20] and a recently proposed model, [21]. The latter requires the electron temperature at the separatrix and in the scrape-off-layer and cannot be compared to experimental data, as such measurements are not available at ASDEX Upgrade with the required accuracy yet. More than two decades ago it has been

suggested by theory, [22], and found in experiment, [23], that the shear of the plasma flow driven by $E \times B$ at the plasma edge can explain turbulence and transport reduction in a developed H-mode. Nowadays this paradigm is largely accepted and indeed, in all toroidal devices, see e.g. review [24], a strong negative well of the radial electric field, E_r, is measured at the very edge of the H-mode plasmas. The flow shear driven by ∇E_r is assumed to reduce the turbulence as observed during the H-mode. The radial electric field at the edge is mainly driven by the ion pressure gradient, in agreement with the neoclassical theory, [25] and references therein. It should be underlined that, despite the fact that ∇E_r is expected to be the actual quantity which impacts on the turbulence, the minimum of the well, $E_{r,min}$, is convenient to characterize the well, because it is more reliably measured in the experiment. As the width of the well is observed to be rather constant in a single device, see e.g. [26, 27], $E_{r,min}$ is representative of ∇E_r and therefore of the effect of the E_r well on the turbulence level. Despite its clear role in a developed H-mode, the contribution of the E_r well in the physics mechanism of the L-H transition itself has not been unambiguously demonstrated so far and the possible need for an additional trigger is often invoked. In the last years, the reduction of turbulence by the self-induced zonal flows (ZFs) and geodesic acoustic modes (GAMs) has been proposed by theory [28] and suggested by several experimental results as a trigger mechanism, [29, 30, 31, 32, 33, 34]. Through this "predator-prey" mechanism a train of limit cycle oscillations, also named intermediate phase (I-phase), is often observed prior to the actual L-H transition. However, the E_r-induced flow shearing prior to the L-H transition should be sufficiently strong to further keep the turbulence at a low level after the action of the trigger and when the ZFs and GAMS disappear because of the reduced turbulence level. Indeed, recent results from ASDEX Upgrade indicate that the E_r well depth just prior to the L-H transition exhibits a constant value over a wide range of densities and temperatures, [35]. As the radial electric field is mainly driven by the main ion pressure gradient, this result is coherent with the fact that a certain power threshold is required for entering the I-phase and triggering the L-H transition. Further investigations, presented below, reveal that the ion heat channel indeed plays a crucial role in the L-H transition.

An overview of the ASDEX Upgrade studies on H-mode physics have been reported in [36]. The present paper is focused on the L-H transition physics and presents new results. It is organized as follows. In the next section the main characteristics of our experiments are described, as well as the diagnostics which are essential for the studies reported in this paper. The results on the impact of the metallic wall on P_{L-H} and the dependence on the ion mass, as well as new results on the plasma current dependence of both the L-H and H-L power thresholds, are presented in section 3. In section 4, we discuss the L-H transition physics mechanism and our results on the role of the ion channel. Finally, based on new experiments, the effect of the MPs on P_{L-H} is described and discussed in section 5, followed by a concluding section.

2. Experimental set-up and diagnostics

ASDEX Upgrade, a divertor tokamak of major radius $R = 1.65$m and minor radius $a = 0.5$m, is equipped in particular with NBI and ECRH heating systems. In the discharges presented here, the ECRH was deposited in the central part of the plasma, $\rho_{tor} < 0.3$, corresponding to a range for the absolute value of B_T between 2.3T and 2.7T which is the window used in the data presented here. Here, ρ_{tor} is the usual normalized toroidal flux radius. In this paper we also use the poloidal flux radius, ρ_{pol}, to display profiles at the edge of the plasma. The ECRH scheme was second harmonic X-mode which provides 100% absorption in the electron channel with a narrow deposition profile. The discharges were all run in a standard ASDEX Upgrade magnetic configuration with the ion ∇B_T drift towards the X-point, i.e the magnetic configuration for a lower P_{L-H}.

ASDEX Upgrade is equipped with all the standard diagnostics of a present-day tokamak. Detailed edge profiles are very important measurements to investigate the L-H physics mechanism and were available for a large part of the discharges used for the present work. The density profiles are provided by the Integrated Data Analysis (IDA) which combines n_e measurements from the lithium beam diagnostic at the edge and the interferometer in the core, [37]. In the following we also use time traces from the DCN line-averaged densities, one of

them is labelled "core" as its corresponding line of sight passes close to the plasma axis, while the other is labelled "edge" and represents a line of sight whose tangency radius is generally close to the $\rho_{tor} \approx 0.8$ flux surface, the geometry details are provided in [38]. We name this quantities $\bar{n}_e$ and $\bar{n}_{e,edge}$ respectively, in which the length taken into account to average the density is the distance along the line of sight between the two points where it crosses the separatrix. The electron temperature is provided by the Thomson scattering diagnostic and a 60 channel electron cyclotron emission (ECE) heterodyne radiometer. For the latter, a forward model within the IDA frame is applied to deduce accurate electron temperature profiles from the measured radiation temperature, [39]. This analysis is particularly important in the edge region with strong gradients. The ion temperature measurement yielded by charge exchange recombination spectroscopy (CXRS) has been very significantly improved since 2011 through an upgrade of the core system, [40], and the installation of two edge systems with viewing cords in both the toroidal and poloidal directions, [41]. The upgrade of the core system enables the measurement of T_i with a 4 ms time resolution on 25 radial core channels while each edge system has 8 radial channels with 2 ms time resolution. In discharges without NBI, e.g. heated by ECRH only, T_i and rotation profiles can be measured with NBI blips of about 10 ms duration, yielding excellent data with a minimal influence on the plasma, [40].

As mentioned above, the actual L-H transition is often preceded by an intermediate phase, labelled I-phase, in which the plasma oscillates between states of low and high transport due to the interaction between turbulence and GAMs, [32]. During the I-phase the edge temperatures and density increase little: the pedestal development is weak. In this paper, however, we keep the label L-H for the transition from the I-phase to the actual H-mode after which a significant reduction of the edge transport induces a sudden increase of the edge density and, to a lesser extent, of the temperatures. In the following, the threshold power values are yielded, as usual, by the loss power, $P_{loss} = P_{heat} - dW/dt$, where P_{heat} includes all the heating contributions, taking into account losses and absorption coefficients of the different heating methods, and W is the plasma energy. Most of the data used in our analysis of P_{L-H} have been obtained in dedicated experiments in which the heating power was ramped

slowly, or increased in small steps, to reduce the largest source of experimental uncertainties which is due to dW/dt. However, some points were taken from other studies in which the dW/dt contribution might be larger. The uncertainties induced by dW/dt are reflected in the error bars. As for the analysis which yielded the ITPA scaling, the radiation losses inside the separatrix are not subtracted. It should be underlined though, that the P_{L-H} analysis is done in L-mode or I-phase time windows of the discharges, where the impurity concentrations are low and the ratio of radiation power in the plasma core to heating power is also rather low and almost independent of the plasma conditions. This is generally not the case for the H-L transition, as discussed in the next section.

3. Power threshold results

3.1. Transition from graphite to tungsten wall

The original graphite plasma facing components in ASDEX Upgrade have been replaced stepwise in time by tungsten-coated elements. This process was started in 2003 and the change was completed in 2007, as described in [10, 11, 12, 13]. Since this date two experimental campaigns (2007-2008) were carried out without boronization, while boronization have been applied regularly after this period. The ASDEX Upgrade threshold data contributed to the ITPA database were, so far, taken from discharges performed during the carbon wall period and are in good agreement with the ITPA scaling, see [42, 2].

Dedicated L-H experiments were carried out in 2008 with the full tungsten wall to investigate the density dependence of P_{L-H}. They revealed that the threshold was about 25% lower than previous data and therefore also below the scaling by the same amount, [14]. This has been confirmed during the following campaigns 2011-2013. This reduction is well documented by the "H-mode standard shot" which is run as the first discharge at the beginning of each experimental day since 1999, [43]. As described in this reference, the H-mode standard shot includes a power ramp to measure P_{L-H} at a density of about $4.5 \times 10^{19}\mathrm{m}^{-3}$ which was in the validity domain of the scaling for ASDEX Upgrade. The H-mode standard shot was

originally developed at $I_p = 1$ MA with $|B_T| = 2$T yielding $q_{95} \approx 3.3$. As the tungsten surface coverage increased, the plasmas were prone to tungsten accumulation in the low power phase following the L-H transition due to the development of an ELM-free phase. This was cured by increasing the value of B_T to 2.5T, corresponding to $q_{95} \approx 4.2$. In parallel, the required density at the L-H transition was increased to $5 \times 10^{19}\mathrm{m}^{-3}$ since shot Nr. 19838. The value $|B_T| = 2.5$ T has been used regularly since 2007, but some discharges run at 2.5T with the carbon wall in 2005-2006 provide a comparison at the same magnetic field between the carbon and tungsten periods. This indicates that the different magnetic field is not the reason for the lower normalized power threshold. This large set of data yields an overview of the evolution of P_{L-H} over the last 12 years which is shown in Fig. 1 where the normalized power threshold P_{L-H}/P_{scal} is plotted versus shot number. The normalized threshold takes into account the slight density variations and the changes in B_T mentioned above. The fraction of tungsten plasma facing components surface is also indicated in the figure.

During the 2007, 2008 and 2009 campaigns the investigation of P_{L-H} could not be carried out regularly due to technical limitations caused by a damaged flywheel generator. The last H-mode standard before this accident was shot Nr. 21388 in April 2006. The regular H-mode standard shots could only be restarted with shot Nr. 25600 in November 2009. This explains the lack of points in this period during which only a few data points could be gathered in dedicated experiments. The averaged value of the normalized threshold is close to unity until 2006 and clearly below, at about 0.75, with full covering with tungsten and after hand-cleaning of all the surfaces during a vessel opening. The larger data scatter with the carbon wall (2001 - 2006) is attributed to the higher sensitivity of graphite to what happened in the previous discharges. An analysis of the scatter with the carbon wall has been presented in [43] and a further discussion is out of the scope of this paper. The data points with 2T and 2.5T are displayed with different symbols indicating that the normalized threshold is, indeed, independent of B_T in this range. It must be underlined that, similarly to the observation made in JET, [16], we verified that the lower power required to induce the L-H transition in the metallic machine is reflected by proportionally lower edge electron temperatures. This is

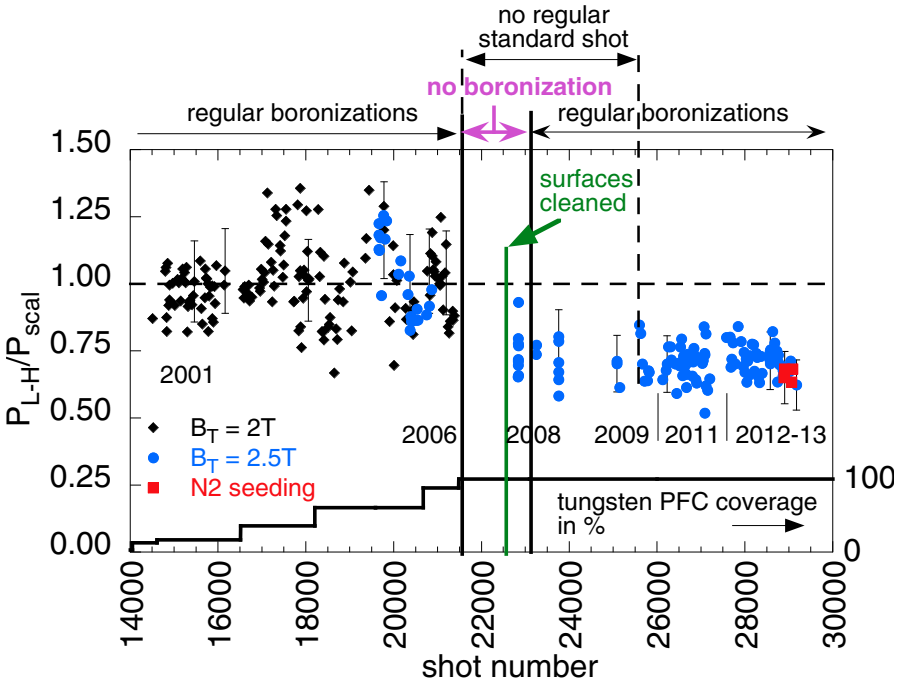

Figure 1. *Power threshold normalized to the ITPA scaling as a function of shot number for the H-mode standard shots, giving an overview of the evolution of the L-H threshold power in ASDEX Upgrade for similar plasma conditions over the last decade. Relevant information of the years is also indicated, there was no campaign in 2010.*

shown in figure 2 for H-mode standard shots run at $|B_T| = 2.5$ T. In panel (a) the electron temperature at $\rho_{pol} = 0.97$ is plotted versus P_{L-H}. As mentioned above, the density has been increased from $\bar{n}_e \approx 4.5 10^{19} m^{-3}$ to $\bar{n}_e \approx 5.0 10^{19} m^{-3}$ during the carbon period, after shot 19838. This is reflected by a slight decrease of $T_e(\rho_{pol} = 0.97)$ for the cases with higher density. Otherwise this plot shows that the edge temperature follows roughly the heating power at the L-H transition and that it is indeed lower with the metallic wall in agreement with the low value of P_{L-H}. To take the differences in density into account, we plot in panel (b) the product $\bar{n}_{e,edge} \times T_e(\rho_{pol} = 0.97)$ where $\bar{n}_{e,edge}$ is deduced from the interferometry channel as described in section 2. For this analysis we prefer this quantity, instead of the local edge density, because it has a very high accuracy in such identical discharges which all have the same plasma shape. This avoids further scatter which would blur the plot. The quantity $\bar{n}_{e,edge} \times T_e(\rho_{pol} = 0.97)$, which we do not refer to as electron pressure because density and

temperature are not measured at exactly the same position, exhibits a clear dependence upon P_{L-H} and is lower for the low threshold values with the metallic wall. This indicates that the lower threshold with the metallic wall is indeed a physics effect which is not due to different radiation losses or changes in the heating power calibration or absorption.

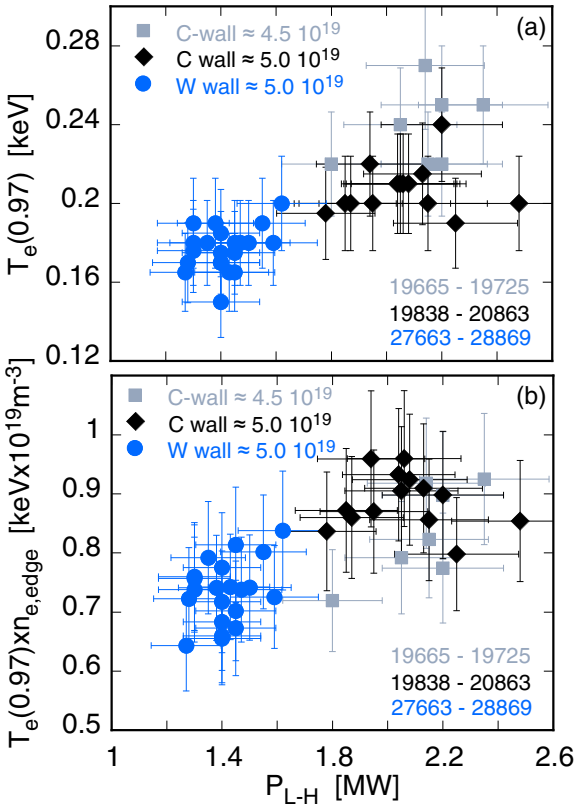

Figure 2. *Effect of the C and W walls on electron edge quantities, all data for* $|B_T| = 2.5$ *T. Plot (a): electron edge temperature at* $\rho_{pol} = 0.97$ *versus* P_{L-H} *for H-mode standard shots with the C and W walls. The change of the density during the C-wall from* $\bar{n}_e \approx 4.5 \times 10^{19} m^{-3}$ *to* $\bar{n}_e \approx 5.0 \times 10^{19} m^{-3}$ *is indicated with different symbols. Plot (b):* $\bar{n}_{e,edge} \times T_e(\rho_{pol} = 0.97)$ *versus* P_{L-H} *for the same data point as in plot (a).*

One may speculate that this decrease of the threshold with the metallic wall is caused by the significant reduction of the carbon concentration. Remarkably, it did not occur gradually which can be attributed to the fact that the reduction of the carbon concentration mainly occurred after the cleaning of the inner wall. Indeed, due to the gradual change from the carbon to the tungsten wall a high level of residual carbon was found on the surfaces before

the cleaning. After the wall cleaning, the carbon concentration was strongly reduced such that the dominant light impurities were carbon, boron and oxygen in concentrations estimated to be well below 0.5 % in the H-mode standard shots prior to the L-H transition. The substantial concentration of carbon with the carbon wall might therefore have increased the L-H threshold through dilution. In this respect, in addition to the results from JET, the reduction of P_{L-H} achieved in NSTX with lithium conditioning, which is a metallic coating on carbon plasma facing components, is worth noting, [44]. Finally, it should be underlined that in the lower power L-modes before the L-H transition, the tungsten concentration is below the detection level of 5×10^{-6}, whereas it can be up to two orders of magnitude higher in usual H-modes. Therefore, neither the core nor the edge tungsten concentrations and the corresponding radiation play any role in the L-H power threshold. This is confirmed by the fact that boronizations have no impact on P_{L-H} in the tungsten wall.

As reported in [35] for ASDEX Upgrade, the edge ion pressure gradient seems to play a key role in the L-H transition physics through its contribution to the radial electric field at the plasma edge, which could be altered by a radially dependent concentration of light impurities in the plasma edge. The diagnostic set available before 2006 does not allow the measurement of the edge radial electric field and we cannot compare data from this period with the carbon wall to our recent results with sufficient accuracy. However, in a recent attempt to mimic the presence of carbon in standard H-modes performed in the tungsten-coated vessel, we injected various amounts of nitrogen before the L-H transition. The injected nitrogen gas flux were, in $10^{21}s^{-1}$, 1, 2, 3, 4 and 6. These points, specifically marked in Fig. 1, do not significantly deviate from the others in the tungsten-coated machine and certainly do not reach the power level of the data measured in the carbon device. The concentration measurement of nitrogen at the L-H transition is affected by large uncertainties, but we estimate that the value reached with a nitrogen flux of $4 \times 10^{21}s^{-1}$ was equivalent to that of carbon before the change to the metallic wall. The maximum nitrogen flux of $6 \times 10^{21}s^{-1}$ produced a disruption before the L-H transition. Obviously, this quantity induced a large concentration which was not realistic to mimic the older carbon concentration for which we never had disruptions in this phase

of such discharges. Thus, we have no direct experimental evidence that the reduction of the carbon concentration is the physics cause of the threshold reduction, but, from our point of view, this seems to be the most probable cause. One may also invoke a reduction of the residual hydrogen concentration associated with the metallic wall. However, considering that the residual hydrogen concentration with the carbon wall was at most 5%, this hypothesis seems unlikely to explain a 25% reduction of P_{L-H}. Finally, we found no evident indication of changes in recycling which could explain this reduction. However, it should be underlined that the L-H transition depends critically on the ion pressure gradient in the very edge of the plasma, a quantity which might react to changes not visible within the uncertainties of the measurements, or be induced by effects occurring in the divertor and scrape-off-layer.

In summary, the reduction of P_{L-H} with a metallic wall compared to a carbon environment is a robust experimental finding, clearly evidenced by our results over several years and confirmed by the recent experiments in JET. As demonstrated by the analysis of the edge data, this effect is directly linked with the transition physics and cannot be attributed to lower radiation losses from the plasma inside the separatrix.

3.2. L-H and H-L power thresholds

The density dependence of the H-mode power threshold has been recognized to be non-monotonic for about two decades, see e.g. [1] and references therein, and has been the subject of recent studies [45, 14, 46]. The threshold exhibits a minimum at $\bar{n}_{e,min}$ which separates the so-called low and high density branches. Only data from the latter were used to derive the ITPA power threshold scaling, Eq. 1, where the condition $\bar{n}_e > \bar{n}_{e,min}$ depends on the device, [2].

For ASDEX Upgrade with the W wall, we found $\bar{n}_{e,min} \approx 4.5 \times 10^{19}\mathrm{m}^{-3}$ for discharges at a plasma current of $I_p = 1$ MA, [14]. These P_{L-H} results have recently been extended with more data at 1.0 MA and with data gained at lower currents of 0.8 MA and 0.6 MA. The variation of the plasma current presented here was motivated by the need to extend the available low density data for various current values. The results are displayed in Fig. 3.

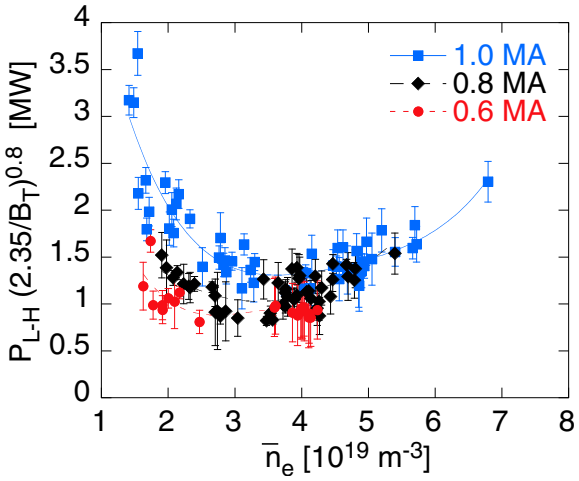

Figure 3. *Power threshold versus density for the L-H transition normalized to* $|B_T| = 2.35$ *T by the* $B_T^{0.8}$ *dependence. The fits to the* P_{L-H} *data indicated here are also shown in Fig. 4. The error bars include all the contributions to* P_{loss}*. The larger error bars are due to the* dW/dt *term for discharges with a rather strong change of heating power before the occurrence of the L-H transition.*

In these data sets, the low density points, below about $4 \times 10^{19}\mathrm{m}^{-3}$, were all obtained with ECRH. As already mentioned above, to take into account the variations of the B_T values (2.3T - 2.7T) around $|B_T| = 2.35$T which is the value for the main part of the dataset, we normalized the power by the $B_T^{0.8}$ dependence of the threshold scaling, taking as reference $|B_T| = 2.35$T. This enables the inclusion of more data points in the analysis. Note that the highest density which can be reached for L-H transition studies is limited by the density limit which is proportional to the plasma current. This explains the different upper boundaries of the high density branch which could be explored at the three plasma current values. Figure 3 indicates a decrease of both $\bar{n}_{e,min}$ and P_{L-H} with decreasing plasma current. The dependence on plasma current occurs only in the low density branch, whereas all data converge towards a common curve in the high density branch of P_{L-H}, in agreement with the fact that no I_p dependence is found in the ITPA threshold database analyses. We will show in the next subsection that this is attributed to the edge ion heat flux in relation with the radial electric field.

We also investigated the threshold power of the H-L back transition, P_{H-L}, plotted versus density in Fig. 4 for the same three I_p values. The fits to the respective P_{L-H} data sets of Fig. 3

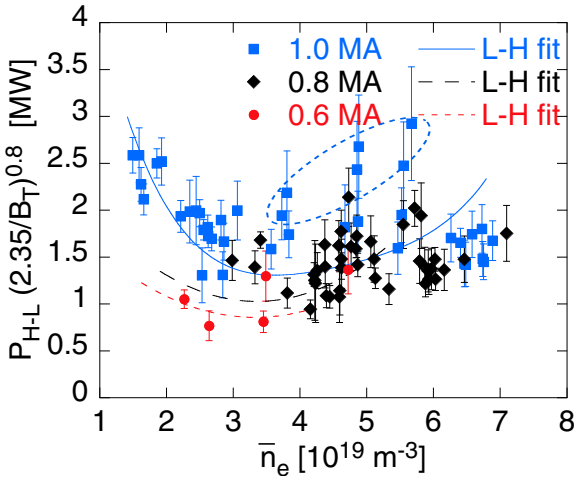

Figure 4. *Power threshold versus density for the H-L transition, normalized to* $B_T = 2.35T$ *by* $B_T^{0.8}$. *The fits to the* P_{L-H} *data are plotted here for comparison between the L-H and H-L thresholds. The error bars include all the contributions to* P_{loss} *where those from dW/dt often dominate.*

are also shown to enable the comparison of P_{H-L} with P_{L-H}. Remarkably, the P_{H-L} data also exhibit a non-monotonic behaviour which is very similar to that of the L-H transition. This is particularly clear for the 1 MA data set which comprises most of the dedicated experiments. A large number of H-L points lie close to or even clearly above P_{L-H} showing that the hysteresis is not a general feature in this representation. In the high density branch only, several points exhibit a clear hysteresis, defined as $P_{H-L} < P_{L-H}$. The lack of hysteresis for the other data above $n_{e,min}$ is mainly due to the radiation losses which generally increase in the H-mode phase and are larger at the H-L transition as compared to the corresponding L-H points. It should be underlined that the increase of the radiative power after the L-H transition is particularly pronounced when the L-H transition occurs in the high density branch. In particular, the points encircled in Fig. 4 exhibit a very high radiation which explains why they lie clearly above the others. Indeed, the L-H transition is known to be linked to the net power through a magnetic surface just inside the separatrix which would then require the radiation losses inside this surface to be subtracted. However, this quantity suffers from a large scatter which induces correspondingly large scatter and uncertainties on the net threshold

values, such that the final results indeed suggest the existence of an hysteresis, but with poor significance. These results are therefore not shown here. Further, it should be underlined that, in the low density branch, the hysteresis can be masked by the strong decrease of the threshold power with increasing density in this window of operation.

Summarizing, the L-H and H-L power thresholds exhibit very similar dependences and the hysteresis often does not appear clearly which is mainly caused by the rather large radiation fraction which develops during the H-mode. This contribution is significantly higher with the tungsten wall, the hysteresis was clearer in the carbon wall [47]. The investigation of the hysteresis at the H-L transition is not the only aspect of this topic which can be extended by the study of the comparison between P_{loss} and P_{scal} during the development of the H-mode after the L-H transition. In fact, after the L-H transition the density generally increases strongly, causing an increase of $P_{scal} \propto \bar{n}_e^{\,0.72}$ which often leads to the situation $P_{loss} < P_{scal}$ if the input power at the L-H transition was close to P_{scal}. However, this does not induce any H-L transition which is a clear sign of hysteresis: the H-mode can be sustained with $P_{loss} < P_{scal}$. This effect is essential in view of ITER where the L-H transition is foreseen to be triggered at $\bar{n}_e \approx 5 \times 10^{19} m^{-3}$, while the actual operation density will be around $10^{20} m^{-3}$.

3.3. Isotope dependence of the power threshold

As mentioned in the introduction, the L-H power threshold is well-known to depend on the ion mass with an M_i^{-1} dependence for the hydrogen isotopes, which is in particular reflected by the fact that the threshold power in hydrogen is about two times higher than in deuterium. In ASDEX Upgrade with the carbon wall, the threshold in hydrogen was about 1.8 times higher than that in deuterium and P_{L-H} in helium was about 40% higher than in deuterium, [14]. With the metallic wall, the thresholds of deuterium and helium are identical over the whole density range, as reported in [14]. Recent investigations of P_{L-H} in hydrogen with the tungsten wall and under the same experimental conditions as those used for the results obtained in D and He, have been conducted. The P_{L-H} results for hydrogen, deuterium and helium with the metallic wall are plotted versus density in Fig. 5.

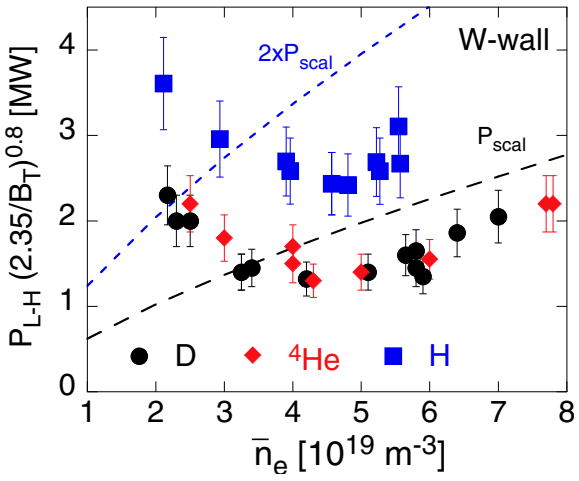

Figure 5. *Power threshold versus density, normalized by the $B_T^{0.8}$ dependence, for deuterium, helium and hydrogen with the tungsten wall. All data from 1MA discharges. $2 \times P_{scal}$ is the ITPA prediction for hydrogen.*

The three gases exhibit the same density dependence with a minimum at about $4.5 \times 10^{19}\mathrm{m}^{-3}$. The threshold power in hydrogen with the metallic wall remains also higher than in deuterium by a factor of 1.8, as with the carbon wall, but its value is then 30% lower than with the graphite wall. Consequently, in the high density branch, the threshold power for hydrogen with the tungsten wall is significantly lower than that predicted by the ITPA scaling, as clearly indicated by the comparison with $2 \times P_{scal}$ used for the extrapolation to ITER. This is quite favorable for the non-nuclear phase.

The helium plasmas of the non-nuclear phase in ITER will contain a certain amount of hydrogen introduced by the hydrogen NBI and possibly pellets used for ELM mitigation. It is therefore important to assess the dependence of P_{L-H} in helium plasmas diluted by hydrogen. Our isotope study yields the results shown in Fig. 6 where the normalized threshold power is plotted versus the helium concentration. The helium concentration, deduced in the divertor region from the D I and He I emissions, is expected to reflect the concentration in the plasma edge, which is relevant for the L-H mechanism. The data points have been obtained from L-H transitions induced by ECRH and hydrogen NBI in the high density branch of the power threshold. A significant increase of the threshold seems to take place for helium

concentrations below 0.8.

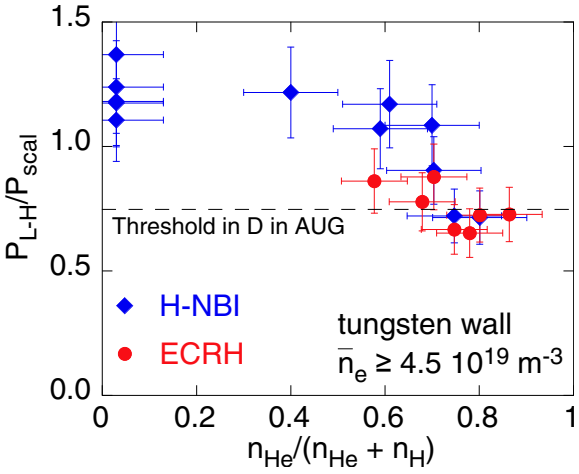

Figure 6. *Normalized power threshold versus helium concentration in a helium-hydrogen plasma. A 3% concentration of helium has been assumed for the "pure" hydrogen plasmas.*

Summarizing, these results are favorable for ITER as they suggest that the threshold power in helium-hydrogen plasmas might remain close to that of deuterium for helium concentrations above 0.8, while in the pure hydrogen plasmas the threshold is only about 1.4 times above the present ITPA prediction for D if the effect of the metallic wall can be extrapolated to ITER.

4. L-H transition physics: Role of the ion channel

The L-H transition and the resulting transport barrier occur at the very edge of the plasma, in a radial radial range of about 2cm inside the separatrix for our discharges, which corresponds to $0.95 \leq \rho_{pol} \leq 1$. The hypothesis that the shear of the plasma flow driven by $E \times B$ at the plasma edge is responsible for the reduction of turbulence and transport in a developed H-mode is widely accepted. In the edge region, where the H-mode transport barrier occurs, the measured negative well of the radial electric field, E_r, is essentially due to the diamagnetic contribution of the main ions, see e.g. [25] and references therein, [48] for measurements in ASDEX Upgrade. In the first approximation one may assume $E_r = \nabla p_i/(e\, n_i)$ where p_i is the

ion pressure, e the elementary charge and n_i the ion density. The flow shearing is then directly linked to ∇E_r and thus to the ion pressure profile.

Therefore, important information in the search for the L-H physics mechanism can be gained through the identification of the respective role of the electron and ion channels. This is possible if, at the time of the L-H transition, the two channels are sufficiently decoupled up to the very edge, such that they can be indeed analyzed separately. This can only be achieved in the low density branch of P_{L-H} and with a heating method which heats dominantly the electrons or the ions. Such a situation has been created in ASDEX Upgrade with ECRH, which exclusively heats the electron channel, [35]. In this study, the minimum of the E_r well at the plasma edge, $E_{r,min}$, has been found to be constant at the L-H transition, independently of the electron density and temperature, at fixed magnetic field. Assuming a constant width of the well, which is a realistic hypothesis, see e.g. [26, 27], this implies that ∇E_r, or equivalently the induced flow shearing is constant at the L-H transition. In reference [35], $E_{r,min}$ has been used because this is a more reliable experimental quantity than ∇E_r. In these experiments, rotation was negligible at the edge such that the E_r was mainly determined by the diamagnetic term of the main ions, $E_r = \nabla p_i/(e\, n_i)$. Therefore these results indicate that the ion heat channel plays a key role in the L-H transition, while the electron channel does not seem to play any role. The following picture for the L-H transition physics emerges. In the usual experimental approach, the L-H transition is induced by a gradual increase of the heating power in the L-mode, with a corresponding increase of the edge ion heat flux, q_i^{edge}. The latter induces a steepening of ∇T_i which, in the edge, leads to an increase of ∇p_i, an enhancement of the E_r well and consequently of the flow shearing. Note that before the L-H transition the density does not change, such that the changes in ∇p_i are only due to the ion temperature induced by the heat flux. In addition, increasing q_i^{edge} tends to enhance the turbulence level and transport might increase, but this also excites zonal flows and/or geodesic acoustic modes, which can transiently reduce turbulence and eventually trigger the L-H transition, [32]. The minimum E_r well value before the L-H transition revealed by the work presented in [35] is necessary to sustain the turbulence suppression by the E_r shearing once ZFs and GAMs disappear as

turbulence is reduced after the L-H transition. In other words, the turbulence suppression triggered by the ZFs and/or GAMs needs a background E_r well to be maintained.

The key role of the ion heat flux also explains the particularly strong increase of P_{L-H} towards low density in ECRH-induced L-H transitions because the edge ion heat flux, for which the only source is the electron-ion collisional energy exchange, $p_{ei} \propto n_e n_i (T_e - T_i)/T_e^{3/2}$, strongly decreases towards low density under such conditions. We deduce the edge ion heat flux from the power balance analysis carried out with the ASTRA transport code [49]. As we investigate here only plasmas with pure electron heating, Ohmic and ECRH, the only source in the ion heat flux channel is provided by the collisional energy exchange flowing from the electron to the ion channel, according to p_{ei}. This effect is calculated with sufficient accuracy as long as the difference $T_e - T_i$ is larger than the experimental uncertainties. This is indeed the case with ECRH and Ohmic heating where $T_e > T_i$ is fulfilled at low collisionality, i.e. in the low density branch. At higher density, T_e and T_i are the same within the experimental uncertainties over a substantial part of the radius in the outer part of the plasma and the electron and ion heat fluxes cannot be separated with sufficient accuracy.

The dependence of P_{L-H} on I_p in the low density branch illustrated by Fig. 3 is linked to the ion heat flux as demonstrated in Fig. 7. The results for the low density region, where the analysis is valid, are shown in Fig. 7 where some representative points from Fig. 3 for P_{L-H} at $|B_T|$ = 2.35T versus density are shown in panel (a) while in panel (b) the corresponding ion edge heat flux values for the points for which the required data are available. We plot here $q_{i,tot}^{edge}$ which is integrated over the flux surface $\rho_{tor} = 0.9$ and provides, in MW, a direct comparison with P_{L-H} shown in panel (a). Note that $q_{i,tot}^{edge}$ is much lower than the corresponding heating power of panel (a). Panel (b) clearly demonstrates that the values of $q_{i,tot}^{edge}$ for 1 MA and 0.6 MA at the L-H transition are consistent, while P_{L-H} at 0.6 MA is lower by at least a factor of 2. This is due to the p_{ei} term under these conditions where mainly T_e varies. Indeed, for a given ECRH power, we observe in these discharges that for 0.6 MA $T_e - T_i$ is larger than for 1.0 MA, whereas T_e itself is lower. These two effects both lead to a stronger electron-ion energy transfer at 0.6 MA and a correspondingly higher $q_{i,tot}^{edge}$.

Therefore, under these experimental conditions at low density, the ECRH power for the 1 MA cases must be higher than at 0.6 MA to provide the required ion heat flux value.

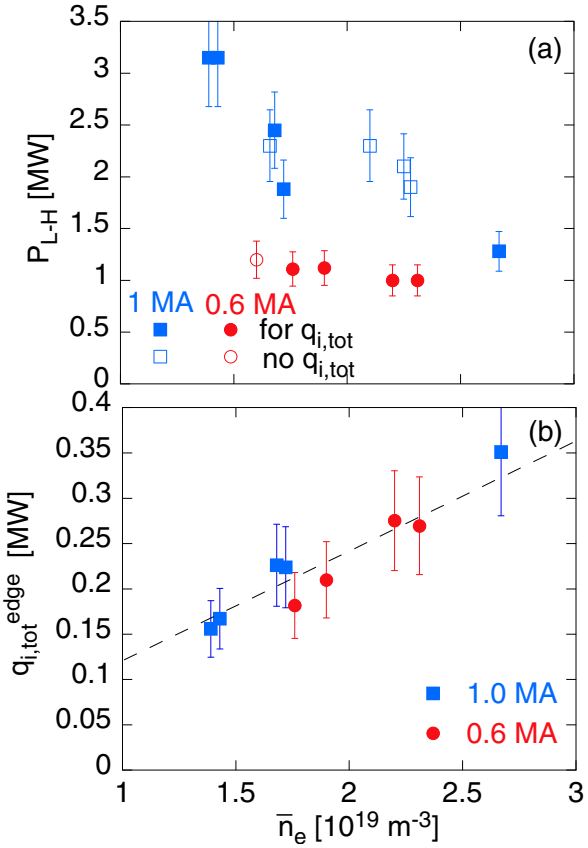

Figure 7. *Panel (a): P_{L-H} versus density for a selection of points from Fig. 3 with $|B_T| = 2.35T$. The closed symbols are the points for which a calculation of the edge ion flux, $q_{i,tot}^{edge}$, can be performed and plotted in panel (b). For the open symbols $q_{i,tot}^{edge}$ cannot be calculated, but they are shown to better illustrate the dependences. Panel (b) shows $q_{i,tot}^{edge}$, at $\rho_{tor} = 0.9$, at the L-H transition, for the closed symbols of panel (a). The dashed line in panel (b) is a linear fit to the data forced through the origin.*

It should also be noted in Fig. 7 that $q_{i,tot}^{edge}$ at the L-H transition increases with density, whereas P_{L-H} decreases, which is explained by the density dependence of the energy exchange term. The flux $q_{i,tot}^{edge}$ at the L-H transition increases about linearly with the density as indicated by the dashed line which is a linear least square fit to the data forced through the origin. A free fit yields almost the same line. Remarkably, this dependence is consistent with that of P_{L-H} in the high density branch: extrapolating $q_{i,tot}^{edge}$ to higher density along the fit

yields for $q_{i,tot}^{edge}$ a value of 0.6MW at $5 \times 10^{19}\mathrm{m}^{-3}$, which is half of P_{L-H} and seems plausible under conditions of rather strong coupling between ion and electron channels.

These results, based on a completely different approach than those published in [35], clearly confirm the key role of the ion heat flux in the L-H transition mechanism through the ion diamagnetic contribution to the E_r well.

Finally, as reported in [50], we found in ASDEX Upgrade that the edge pressure profiles at the H-L transition are very similar to those at the L-H transition indicating that the E_r profile at the back transition is close to that at the L-H transition, also emphasizing the key role of this quantity in the transition physics. The reader is referred to [50, 36] for more details.

5. L-H transition in the presence of magnetic perturbations

One promising method to mitigate the power load released by the ELMs is offered by applying non-axisymetric magnetic field perturbations, labelled here MPs, using adequate saddle coils. This indeed enables H-modes with very small or even completely suppressed ELMs to be run, [51, 52, 53, 17, 54]. Since 2011 ASDEX Upgrade is equipped with such saddle coils, named B-coils, which can produce perturbations with $n \leq 4$, where n is the toroidal mode number. We used n=2 in the present work. A specific feature of the ELM mitigation with MPs in ASDEX Upgrade is that it occurs at rather high plasma density, [54], above a value labelled $n_{e,mitig}$, which corresponds typically to 65% of n_{GW}, the Greenwald density. This effect does not depend on whether the MP configuration is resonant or non-resonant.

As accessing the H-mode in ITER with the foreseen heating power will be crucial, it is essential to investigate the effect of the magnetic perturbations on the L-H transition and P_{L-H}. Results have been obtained in MAST [17], DIII-D [6], NSTX [18], using an n=3 setting for the MPs. These results all indicate an increase of P_{L-H} with the amplitude of the applied perturbation, which can be as high as two times above the P_{L-H} value without MPs.

Similar experiments have been conducted in ASDEX Upgrade, [19]. Their goals were to achieve transitions to H-mode without a single large ELM, i.e. full avoidance of type-I ELMs, and to assess the effect of the MPs on P_{L-H}. It turned out that the MPs do not affect the L-H

transition for $\bar{n}_e < 0.45 n_{GW}$ while for $\bar{n}_e > 0.65 n_{GW}$ no L-H transition could be achieved with heating powers as high as two times the usual P_{L-H} value. In the intermediate density range, small ELMs were obtained right after the L-H transition while P_{L-H} was increased by only 20%, [19]. First results presented in this reference suggested that the increase of P_{L-H} is due to a flattening of the edge pressure profiles by the presence of the MPs, but this remained to be assessed. This preliminary statement has been confirmed in recent experiments in which we could investigate more accurately the impact of the MPs on the edge profiles, as described in the following.

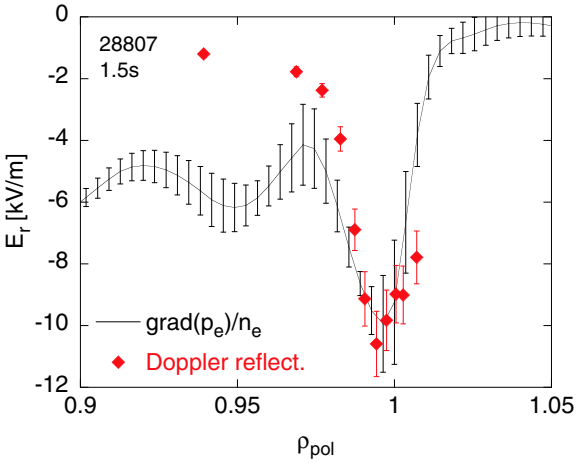

Figure 8. *Comparison of the edge E_r profiles deduced from Doppler reflectometry and $\nabla p_e/(e\, n_e)$.*

As already mentioned, there are convincing experimental indications that the E_r well must be sufficiently pronounced for the L-H transition to occur [35]. As indicated in the introduction, the relevant physics parameter for turbulence reduction is the sheared flow which is driven by ∇E_r, but this gradient is generally not measured with sufficient accuracy, whereas the minimum of the well, $E_{r,min}$, is better determined and therefore used to characterize the edge E_r well. We also follow this approach in this section. The analysis of the E_r field deduced from the CXRS data requires detailed profiles at the very edge of the plasma which, with our present systems, can only be obtained if the plasma is scanned radially by about 1cm to increase the radial resolution. This movement requires about 200ms and is not adequate

to study the L-H transitions under the conditions used here. Indeed more discharges than available would have been needed to produce long enough L-mode phases at a heating power just below P_{L-H}. As indicated in [35], at densities above $4 \times 10^{19}\mathrm{m}^{-3}$ the T_e and T_i profiles are very similar in the edge plasma, such that, in a first approximation, T_e can be used instead of T_i which allows us to estimate E_r from $\nabla p_e/(e\,n_e)$ with a good time resolution. For this purpose the ECE data were analyzed with the forward modelling method to provide the best possible accuracy of T_e in the edge, [39]. For this analysis the original temperature and density data, which are sampled with a frequency of several kHz, are averaged over 1ms which is also the time resolution of the resulting data and sufficient to investigate the effect of the MPs on the L-H transition. The Doppler reflectometry in ASDEX Upgrade also provides edge E_r profiles, [55, 32]. A profile requires a frequency scan which takes about 100ms, a time resolution which is often not sufficient for the purpose of the present work. However we could cross-check the results delivered by the Doppler reflectometry and those deduced from $\nabla p_e/(e\,n_e)$ for a few cases. An example is shown in Fig. 8 for an L-mode time interval shortly before the L-H transition and during which the plasma parameters varied little. The agreement between the two measurements is good for the outer region, $\rho_{pol} > 0.97$, and in particular for the minimum which gives confidence in the estimate of E_r deduced from $\nabla p_e/(e\,n_e)$. Further inside, $\rho_{pol} < 0.97$, the contribution from toroidal rotation increases and the diamagnetic term does not represent well the E_r profile which explains the discrepancy between the Doppler reflectometry and the $\nabla p_e/(e\,n_e)$ data. More details on this comparison can be found in [56]. For the results presented here, we induced two L-H transitions, one without and one with MPs, under otherwise identical conditions, either in the same discharge with two heating pulses, or in two subsequent discharges. As already indicated above, we used the non-resonant n=2 MP configuration, but we verified that the resonant n=2 configuration yielded very similar P_{L-H} values.

An example is illustrated in Fig. 9 for two discharges in which the L-H transition has been induced in each of them by an identical ECRH pulse. In one discharge the MPs were not activated (28394) and in the other one (28395) the MPs were turned on with the usual

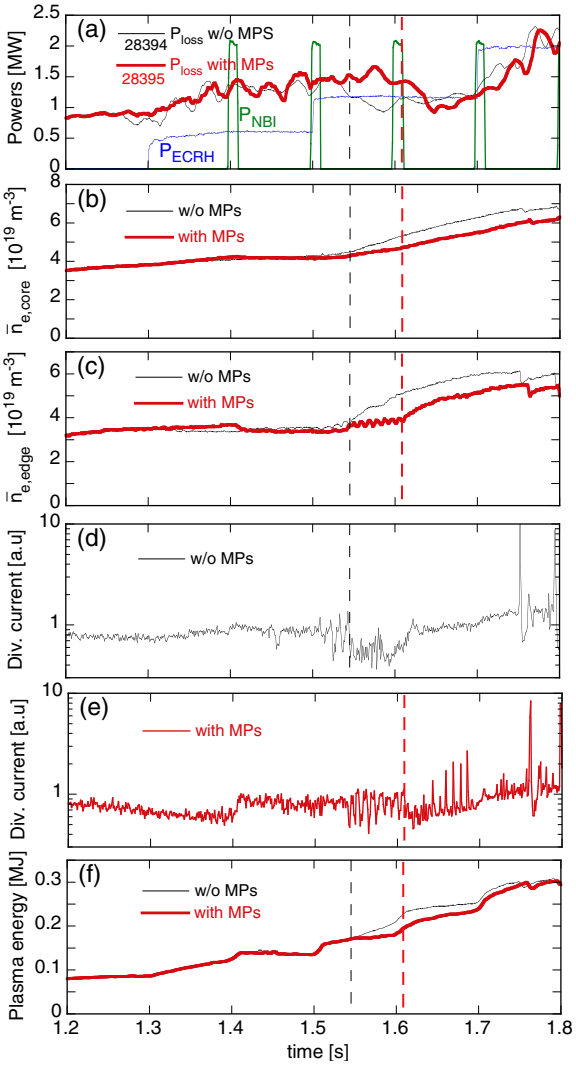

Figure 9. *Time traces of two discharges without MPs (28394) and with MPs (28395). Panel (a) heating powers, (b) and (c) core and edge line-averaged densities respectively, (d) and (e) divertor currents as monitor for L-H transitions and ELMs, without and with MPs respectively, (f) plasma energy.*

maximum coil current of 1 kA. Several signals are plotted in Fig. 9 for each of these two discharges in a time interval around the L-H transition. Beam blips were used to also provide information on T_i to indeed verify that T_e and T_i are similar at the edge, [56]. The L-H transitions, indicated by vertical dashed lines in the plots are well identified by the sudden increase of the edge density, panel (c), and by the drop of the divertor current, panels (d) and (e). The powers plotted in panel (a) indicate that more ECRH power and therefore

somewhat higher P_{L-H} is required in the presence of the MPs. The difference in P_{L-H} is about 15%, which is in agreement with our previous results considering that $\bar{n}_e \approx 0.52 n_{GW}$ in these discharges. As shown by Fig. 9 panel (d), for the case without MPs a clear and rather long ($\approx$ 150ms) ELM-free phase develops until the occurrence of the first type-I ELM which is clearly indicated by a large positive spike in the divertor current. In the case with MPs, the discharge exhibits several type-III ELMs after the L-H transition, which are followed by an ELM-free phase which starts just after the last ECRH step and ends with the first type-I ELM which occurs only slightly later in time than in the discharge without MPs. Consequently, the density at the onset of the first ELM is somewhat lower in this discharge. Note that at the end of this initial time evolution the plasma energy, panel (e), is the same for the two discharges which therefore have the same confinement time.

The T_e, n_e and $\nabla p_e/(e\, n_e)$ profiles for the discharges of Fig. 9 are plotted in Fig. 10 for the relevant time points which are: the L-H transitions of the two discharges, as well as the L-mode time point of the discharge with MPs at the time of the L-H transition of the other discharge, i.e. at the same heating power and density. The errors bars indicated in the figure represent the statistical noise of the data. They are deduced, for each radial position, from the standard deviation (σ) of the data points calculated over a time interval of 10 ms before each corresponding time point. The error bars in the plots represent $\pm\sigma$. Choosing a time interval of 5 or 20 ms to calculate σ yields very similar uncertainties. These error bars do not take systematic uncertainties into account which is justified by the fact that the data are gained from identical discharges using the same diagnostic settings and the same analysis. In pedestal studies one cannot rely solely on the nominal position of the separatrix and the radial position of the different measurements, here T_e and n_e, must be sometimes slightly adjusted. The procedure used at ASDEX Upgrade, described in details in [57], relies on the characteristics of the separatrix. One assumes $T_e = 100 \pm 20$ eV at the separatrix. For the density, the maximum curvature of the density profile at the foot of the pedestal is assumed to be very close to the separatrix, generally about 2 mm outside of it. In the discharges discussed here no radial adjustment was necessary between the 2 measurements. As the ECE and Lithium beam

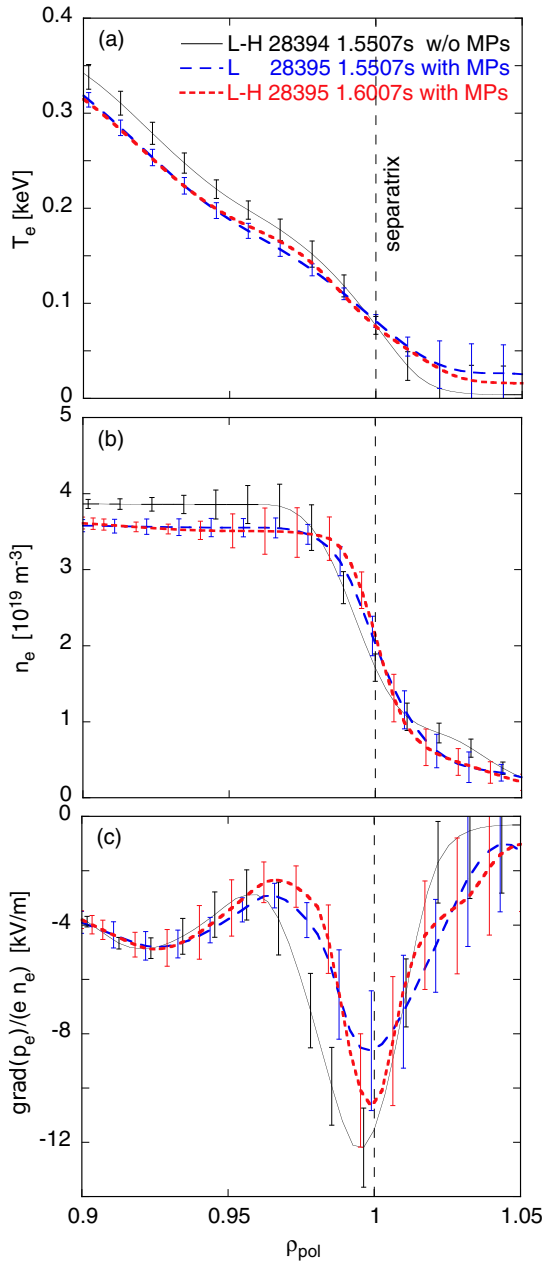

Figure 10. *Profiles with and without MPs at three time points: L-H without MPs and for comparison L-mode at same time with MPs, finally L-H with MPs. Panels (a) electron temperature, (b) density and (c) radial electric field estimates from electron pressure gradient.*

diagnostics are in the same sector of the torus, the effect of the MPs is almost the same and no relative shift between the two diagnostics was required. As the radial position corresponding to $T_e = 100$ eV was close to the nominal separatrix, no correction was done either due to the presence of the MPs. The T_e, n_e and $\nabla p_e/(e\, n_e)$ profiles are shown in Fig. 10. In panel (a), the T_e profiles at the L-H transition without MPs and at the corresponding L-mode time point with MPs exhibit differences which are outside of the experimental uncertainties: the T_e profile with MPs is somewhat flatter inside the separatrix. The large error bars outside of the separatrix reflect the fact that T_e is very poorly determined in this region, see [56]. At the L-H transition with MPs, which requires more heating power, the T_e profile approaches that of the L-H transition without MPs, in particular ∇T_e just inside the separatrix is the same. The density profiles displayed in panel (b) are the same within the uncertainties. The panel (c) indicates the corresponding $\nabla p_e/(e\, n_e)$ profiles, as estimate for E_r. For the case without MPs the E_r well has a minimum at -12 kV/m which is very close to the value of -15 kV/m reported in [35]. For the corresponding L-mode point with MPs, the E_r well is clearly less pronounced and the difference with respect to the same time point in the discharge without MPs is larger than the error bars. For the L-H transition with MPs the E_r minimum reaches -10 kV/m and the well depth is therefore somewhat less pronounced than in the case without MPs but the difference is just at the border of the error bars.

In summary, under the conditions of these experiments, the presence of the MPs seems to mainly flatten the edge temperature profile such that a higher power is required to restore the pressure gradient necessary to induce the L-H transition.

This E_r analysis has been applied to several discharges for both the start of the I-phase and the L-H transition. The results are shown in Fig. 11. These data points could be partially cross-checked by a comparison with the results from Doppler reflectometry, [56]. The range in heating power at the L-H transition, 1.1 to 1.9 MW, has been obtained by variations of density and magnetic field. The values of $E_{r,min}$ for the L-H transitions range between -8 kV/m and -12 kV/m. This is somewhat weaker than the -15 kV/m reported in [35], but not inconsistent with it considering the uncertainties linked with the different analyses and

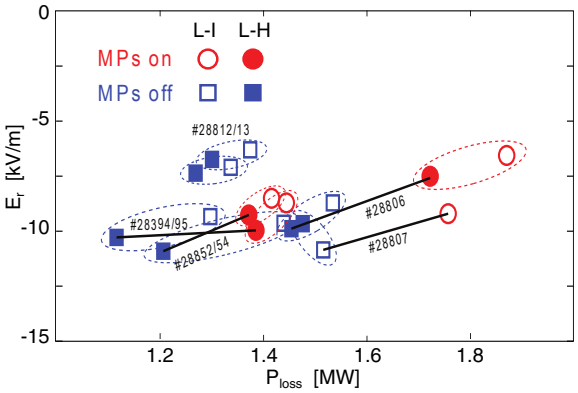

Figure 11. *E_r minimum versus heating power for several discharges. The data were taken at the transitions to the I-phase (L-I) and to the H-mode (L-H) with and without MPs. The points for corresponding L-I and L-H transitions are encircled. The points from discharges with and without MPs run under the same experimental conditions are linked with a line segment and labeled with the corresponding shot number.*

possible experimental differences between discharges carried out under somewhat different conditions in experimental campaigns separated by about 2 years of time. At the onset of the I-phases the E_r well is somewhat less pronounced than for the following L-H transition but the heating power is somewhat higher, as indicated by the encircled pairs of points in figure 11. This is due to the fact that during the I-phase the weak but visible development of the pedestal induces an increase of dW/dt which reduces P_{loss} at the actual L-H transition. Note that this reflects the hysteresis in power.

Summarizing, our study confirms that both the L-I and L-H transitions in the presence of the MPs occur at higher heating powers. This seems to be due to a flattening of the edge ion temperature profile induced by the presence of the magnetic perturbation and reflected in our study by a weaker T_e gradient. In the presence of MPs, the transitions seem to occur for a somewhat less negative $E_{r,min}$ value, which might be compensated by a narrower well width inducing a stronger ∇E_r. This speculation cannot be confirmed with the present data due to the large error bars on ∇E_r but should be the subject of future investigations. The L-I transition points exhibit a somewhat less negative $E_{r,min}$ than the associated L-H points which is in agreement with the development of the E_r well during the I-phase, [32].

6. Summary and conclusion

We have presented recent results obtained in ASDEX Upgrade on the L-H transition threshold and physics. The H-mode power threshold has decreased by about 25% in the change from the graphite to the tungsten wall. This happens for both hydrogen and deuterium such that the threshold in hydrogen remains 1.8 times higher than in deuterium, as observed with the carbon wall. The transition to the metallic wall might also be the reason for the fact that the threshold in helium has been reduced to that of deuterium, but the dataset does not allow a definitive assessment of this assumption. Our study yields the important result that the non-monotonic density dependence of the power threshold is the same for the three gases. Furthermore, our experiments in deuterium indicate that both the minimum power threshold and the density value at which it occurs decrease with plasma current. This affects mainly the low density branch while at high density the dependence on plasma current disappears. The power at the H-L back transition exhibits the same non-monotonic density dependence and the plasma current dependence as well. The physics analysis of the plasma current dependence indicates that it can be attributed to the key role played by the ion heat flux at the plasma edge in the L-H transition mechanism. Therefore, this confirms the results from our previous investigations, [35], which revealed that the well of the radial electric field at the edge, which is mainly driven by the ion diamagnetic contribution, must reach a sufficient depth for the L-H transition to occur. As the width of the E_r well exhibits weak variation, its minimum can be considered as a convenient approximation for the poloidal flow shearing driven by ∇E_r, which is thought to be the actual physics quantity causing the turbulence reduction. We have shown that the required minimum of the E_r well also determines the L-H transition when magnetic perturbations are applied. At a given heating power, the presence of the magnetic perturbations flattens the edge temperature profiles, leading to a weaker E_r well. The required condition for the L-H transition can then be restored by increasing the heating power. Whether the flattening of the edge gradients is due to a transport change or other effects is out of the scope of this paper.

Further dependences of the L-H threshold might be due to changes in the E_r well but have

not be confirmed so far. We have very preliminary indications that the high power threshold in hydrogen might be linked to the high ion heat transport which leads to a weaker edge gradient of the ion temperature than in deuterium at a given edge ion flux, but this still requires assessment. So far, we have not been able to answer the question of whether the different L-H threshold powers with the carbon and tungsten walls correspond to differences in the E_r profiles or not. The analysis of the electron kinetic data at the L-H transition demonstrates that this cannot be attributed to the radiation losses. A continuation of the experiments with impurity seeding before the L-H transition accompanied by accurate measurement of E_r is envisaged.

Finally concluding for future devices, the lower threshold obtained with the metallic wall, also found for hydrogen, is favorable for ITER. In particular for the non-nuclear phase this suggests that P_{L-H} might be significantly lower than predicted by the present ITPA threshold scaling. Along the same line, if the reduction of the threshold in helium to the deuterium level with metallic wall would be confirmed in JET, non-nuclear studies in ITER could be envisaged with more confidence. Obviously, an analysis of the impact of the new ASDEX Upgrade and JET threshold data in deuterium with the metallic walls on the ITPA scaling seems highly desirable.

Acknowledgement

The excellent support of the ASDEX Upgrade technical staff is warmly acknowledged. M. Willensdorfer is a Fellow of the Friedrich Schiedel Foundation for Energy Technology. The views and opinions presented in this work do not necessarily reflect those of the European Commission.

References

[1] RYTER, F. et al., Nuclear Fusion **36** (1996) 1217.

[2] MARTIN, Y. R. et al., Journal of Physics: Conference Series **123** (2008) 012033.

[3] RIGHI, E. et al., Nucl. Fusion **39** (1999) 309 .

[4] GOHIL, P. et al., Assessment of the h-mode power threshold requirements for iter, in *Proc. of the 24rd*

IAEA Fusion Energy Conference, San Diego, USA, volume IAEA-CN-197, pages ITR/P1–36, Vienna, 2012, IAEA, in preparation for Nucl. Fus.

[5] ANDREW, Y. et al., Plasma Physics and Controlled Fusion **46** (2004) A87.

[6] GOHIL, P. et al., Nuclear Fusion **51** (2011) 103020.

[7] MEYER, H. et al., Nuclear Fusion **51** (2011) 113011.

[8] MA, Y. et al., Plasma Physics and Controlled Fusion **54** (2012) 082002.

[9] GOHIL, P. et al., Journal of Physics: Conference Series **123** (2008) 012017.

[10] NEU, R. et al., Journal of Nuclear Materials **363-365** (2007) 52.

[11] NEU, R. et al., Journal of Nuclear Materials **367–370** (2007) 1497.

[12] SIPS, A. C. C. et al., Plasma Physics and Controlled Fusion **50** (2008) 124028.

[13] NEU, R. et al., Plasma Physics and Controlled Fusion **53** (2011) 124040.

[14] RYTER, F. et al., Nuclear Fusion **49** (2009) 062003.

[15] NEU, R. et al., Journal of Nuclear Materials **438, Supplement** (2013) S34 .

[16] MAGGI, C. et al., The H-mode threshold in JET with the ITER-like wall, in *Europhysics Conference Abstracts (CD-ROM, Proc. of the 39th EPS Conference on Plasma Physics 2012 (EPS 2012) and 16th International Congress on Plasma Physics, Stockholm, Sweden)*, volume 36F, page O3.108, Mulhouse, 2012, European Physical Society.

[17] KIRK, A. et al., Plasma Physics and Controlled Fusion **53** (2011) 065011.

[18] KAYE, S. et al., Nuclear Fusion **51** (2011) 113019.

[19] RYTER, F. et al., Nuclear Fusion **52** (2012) 114014.

[20] CONNOR, J. W. et al., Plasma Phys. Controlled Fusion **42** (2000) R1.

[21] FUNDAMENSKI, W. et al., Nuclear Fusion **52** (2012) 062003.

[22] BIGLARI, H. et al., Phys. Fluids B **2** (1990) 1.

[23] GROEBNER, R. J. et al., Phys. Rev. Lett. **64** (1990) 3015.

[24] WAGNER, F., Plasma Physics and Controlled Fusion **49** (2007) B1.

[25] STROTH, U. et al., Plasma Physics and Controlled Fusion **53** (2011) 024006.

[26] GOHIL, P. et al., Nuclear Fusion **38** (1998) 93.

[27] MCDERMOTT, R. M. et al., Physics of Plasmas **16** (2009) 056103.

[28] KIM, E.-J. et al., Phys. Rev. Lett. **90** (2003) 185006.

[29] MOYER, R. A. et al., Phys. Rev. Lett. **87** (2001) 135001.

[30] COLCHIN, R. J. et al., Phys. Rev. Lett. **88** (2002) 255002.

[31] PUNZMANN, H. et al., Phys. Rev. Lett. **93** (2004) 125003.

[32] CONWAY, G. D. et al., Phys. Rev. Lett. **106** (2011) 065001.

[33] ESTRADA, T. et al., Phys. Rev. Lett. **107** (2011) 245004.

[34] SCHMITZ, L. et al., Phys. Rev. Lett. **108** (2012) 155002.

[35] SAUTER, P. et al., Nuclear Fusion **52** (2012) 012001.

[36] WOLFRUM, E. et al., Plasma Physics and Controlled Fusion **54** (2012) 124002.

[37] FISCHER, R. et al., Fusion Science and Technology **58** (2010) 675.

[38] MLYNEK, A. et al., Review of Scientific Instruments **81** (2010) 033507.

[39] RATHGEBER, S. K. et al., Plasma Physics and Controlled Fusion **55** (2013) 025004.

[40] MCDERMOTT, R. M. et al., Plasma Physics and Controlled Fusion **53** (2011) 124013.

[41] VIEZZER, E. et al., Review of Scientific Instruments **83** (2012) 103501.

[42] RYTER, F. et al., Plasma Physics and Controlled Fusion **44** (2002) A415.

[43] RYTER, F. et al., Plasma Physics and Controlled Fusion **44** (2002) A407.

[44] MAINGI, R. et al., Nuclear Fusion **50** (2010) 064010.

[45] ANDREW, Y. et al., Plasma Physics and Controlled Fusion **48** (2006) 479.

[46] MA, Y. et al., Nuclear Fusion **52** (2012) 023010.

[47] RYTER, F. et al., Plasma Phys. Controlled Fusion **36 Suppl (7)A** (1994) A99.

[48] VIEZZER, E. et al., Nuclear Fusion **53** (2013) 053005.

[49] PEREVERZEV, G. V. et al., Max-Planck-Institut für Plasmaphysik, report IPP 5/98 (2002) .

[50] WILLENSDORFER, M. et al., Nuclear Fusion **52** (2012) 114026.

[51] HENDER, T. et al., Nuclear Fusion **32** (1992) 2091.

[52] EVANS, T. E. et al., Nuclear Fusion **45** (2005) 595.

[53] LIANG, Y. et al., Phys. Rev. Lett. **98** (2007) 265004.

[54] SUTTROP, W. et al., Phys. Rev. Lett. **106** (2011) 225004.

[55] SCHIRMER, J. et al., Nuclear Fusion **46** (2006) S780.

[56] RATHGEBER, S. K., "Electron temperature and pressure at the edge of ASDEX Upgrade plasmas", PhD Thesis Ludwig-Maximilian University, Munich, (2013).

[57] SCHNEIDER, P. A. et al., Plasma Physics and Controlled Fusion **54** (2012) 105009.